Precision and Scaling in Morphogen Gradient Read-out

Aitana Morton de Lachapelle and Sven Bergmann*

Department of Medical Genetics, University of Lausanne, 1005 Lausanne
and Swiss Institute of Bioinformatics, Switzerland

*: corresponding author: Sven.Bergmann@unil.ch (+41 21 692 5452)

Supporting Information

Image analysis and control experiments

Scaling models

Image analysis and control experiments

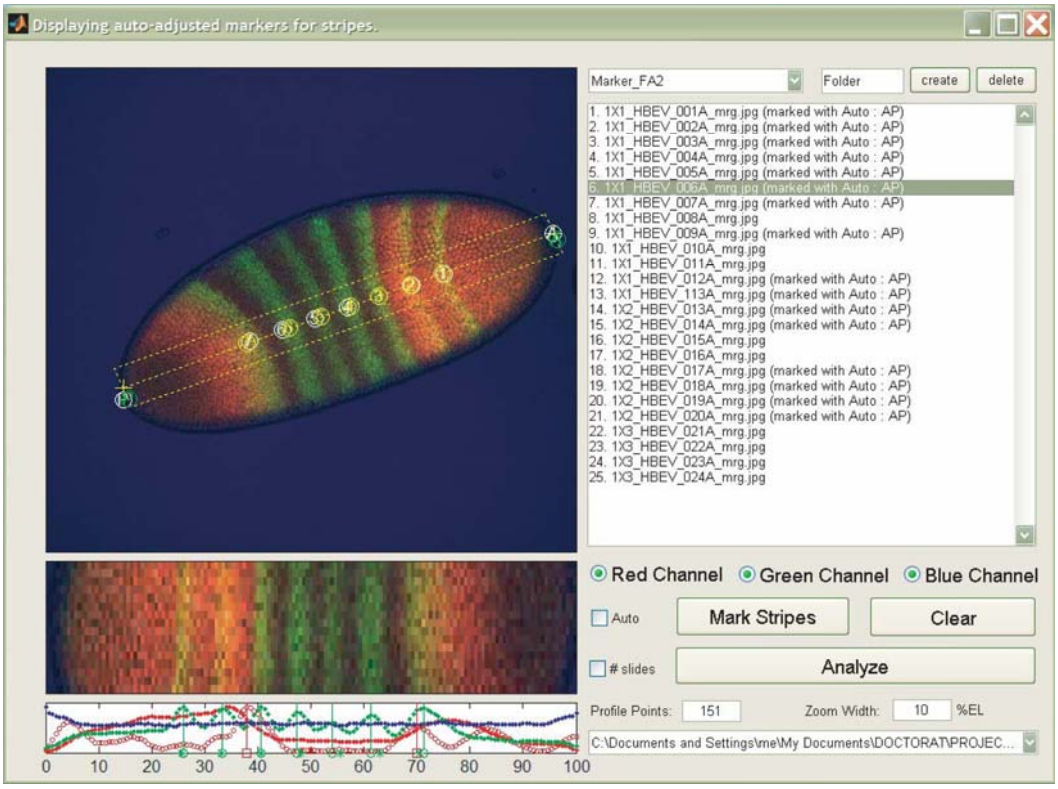

Figure S1. Graphical user-interface for analysis of the gap and even-skipped gene expression domains. The three color profiles (green: Eve stripes, red: Hb, Gt or Kr, blue: background) are extracted for every embryo and shown below the main embryo image. Once all the embryos have been marked, the data can be analyzed, returning precision and scaling features over all the embryos and for a wide range of positions in the embryo.

Text S1. *Statistical significance of the precision and scaling results.*

Our analysis of the gap and pair-rule gene expression domain boundaries showed that precision is highest at mid-embryo (c.f. Figure 1). However, position-dependent precision may also arise as an experimental artifact when analyzing embryos with different orientations (Surkova et al, 2008). At mid-embryo, this effect is the smallest, which could explain at least part of the observed dip in the precision profile (Figure 1). In our analysis, we measured expression profiles close to the line connecting the anterior and posterior pole, where the impact of the embryo orientation is the smallest. We performed a control experiment where expression profiles were extracted 50 times moving uniformly from the top of the embryo (above the AP line) to its bottom (below the AP line). We found that the positional variations induced by this (extreme) procedure were indeed smallest at mid-embryo (Figure S2). Nevertheless, for all seven Eve stripes we found that the median intra-embryo variation (across these 50 extractions) was below the inter-embryo variation we measured. Thus, while we cannot exclude that part of the observed positional dependence of precision is due to our experimental procedure, we find it unlikely to explain it entirely. In particular, it can hardly account for the relatively strong increase of positional fluctuations towards the anterior pole, which is the strongest signature of models with pre-steady state decoding.

A second potential systematic error could be due to the fact that the posterior gap gene expression domains exhibit significant drift towards the anterior pole in cleavage cycle 14 (see Figure 1 in (Jaeger *et al*, 2004)). Apparently, such a drift is also transmitted to the Eve expression domains, where it is strongest (~5%L) for stripe 7 (see Table 1 in (Surkova et al, 2008)). This is relevant because our staining images were taken in time

classes T5-T8 of cycle 14 (based on the fact that the Eve expression domains have been clearly separated) and part of the observed positional fluctuations $\sigma(x/L)$ may be a result of combining data from different time classes. Yet, even for stripe 7, this effect may at best contribute half of the observed variance, while it cannot account for the increased imprecision we observed for the more anterior expression domains (see Figure S3).

In Figure S4, we show the residual variance when substracting the variance due to changes in embryo orientation *and* domain drifts (negative values are set to zero). In order to test for the statistical significance of position dependence in this residual variance, we performed two linear regressions: one with the data of stripes 1 to 4, and a second with the data of stripes 4 to 7. We find that the increase in precision from the anterior pole towards mid-embryo is still highly significant with a p-value < 0.0018. In contrast, while we also observe a trend of increasing precison towards mid-embryo from the posterior pole, this effect is not very significant (p < 0.2) when using the corrected variance. Thus within this very conservative estimate of the residual positional variance, we cannot rule out that the larger contributions towards the posterior pole mainly stem from averaging signals of embryos with different orientation and domain drifts. Nevertheless, we note that the positional increase towards the anterior pole by itself favors the pre-steady state decoding of Bcd within our modeling framework. This is because such an increase can only be driven by noise in the production rate (see Figure 3A) or nuclear binding (Figure 3D) at early times, before the gradient has reached steady state.

The other important conclusion drawn from our image analysis is the hyper-scaling of anterior-most domains. Given the large error bars for these domains, we performed a nested model analysis in order to investigate the statistical significance of this conclusion (Figure S5). Our first model is a simple regression $S = wmean$, where $wmean = \dfrac{\sum_i \left(\frac{1}{\sigma_i^2}\right) \cdot S_i}{\sum_i \left(\frac{1}{\sigma_i^2}\right)}$ is the weighted mean of the scaling coefficients (with σ_i the standard error of the scaling measurement S_i). This model is nested within our second model $S = wmean + \beta(x - x_0)(x < x_0)$ which accounts for hyper-scaling of domains localized at $x \in [0; x_0]$ (note that the estimate of the slope, β, is obtained taking into account the standard errors of the scaling measurements). Because the second model has more parameters than the first one, it will always fit the data better. Thus, in order to determine if the second model gives a *significantly* better fit to the data, we make use of an ***F*** test.

The ***F*** statistic is given by $F = \dfrac{\left(\frac{RSS_1 - RSS_2}{p_2 - p_1}\right)}{\left(\frac{RSS_2}{n - p_2}\right)}$, where RSS_i is the weighted residual sum of squares of model *i*, p_i the number of parameters of model *i* and *n* the number of data points used to estimate the parameters of both models. Under the null hypothesis, the second model does not provide a signicantly better fit than the first model and ***F*** will have an ***F*** distribution with $(p_2 - p_1; n - p_2)$ degrees of freedom. In Figure S5, we see that the null hypothesis was rejected with a p-value < 0.00021. Therefore, despite the big error bars in our measurements, the fact that all the anterior measurements ($x < x_0$ with $x_0 = 40\%L$) show hyper-scaling is still a significant result.

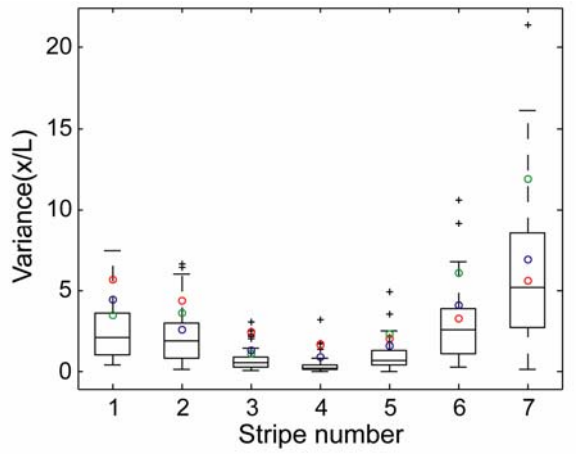

Figure S2. **Contribution of embryo orientation to the variance of the Eve stripes.** Measured variance of the Eve stripes (◦) co-stained with Hb (red), Kr (green) and Gt (blue), for wild-type *bcd* mRNA dosage (c.f. Figure 1). In the control experiment, expression profiles in a given embryo were extracted 50 times moving uniformly from the top of the embryo (above the AP line) to its bottom (below the AP line), giving an (over-)estimate of the maximal positional variance induced by embryo orientation. This was repeated for all embryos in our dataset with wild-type *bcd* mRNA dosage. Thus, the boxplot represents the distribution of positional variabilities due to embryo orientation.

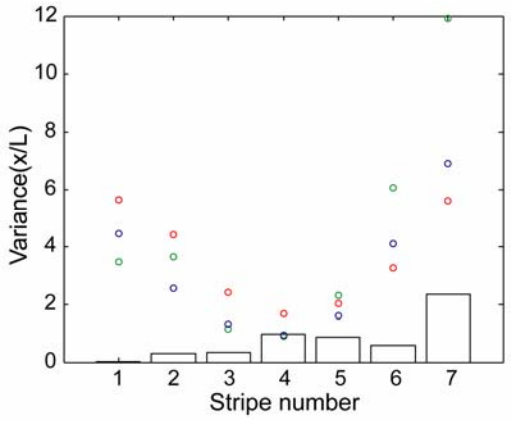

Figure S3. Contribution of domain drift to the variance of the Eve stripes. Measured variance of the Eve stripes (◦) co-stained with Hb (red), Kr (green) and Gt (blue), for wild-type *bcd* mRNA dosage (c.f. Figure 1), together with the estimated maximal variances (bars) that could arise due to the drifts of these domains. These estimates were computed as $d_i^2/12$, i.e. the variance of a uniform distribution between 0 for images taken early (T3 for stripes i=1,2,3,4,7 and T4 for stripes i=5,6) and the maximal drift d_i for images of the last time class T8 (c.f. Table 1 of (Surkova *et al,* 2008)). These are upper bounds since our images were likely taken in T5-T8 based on the differentiation of the Eve domains.

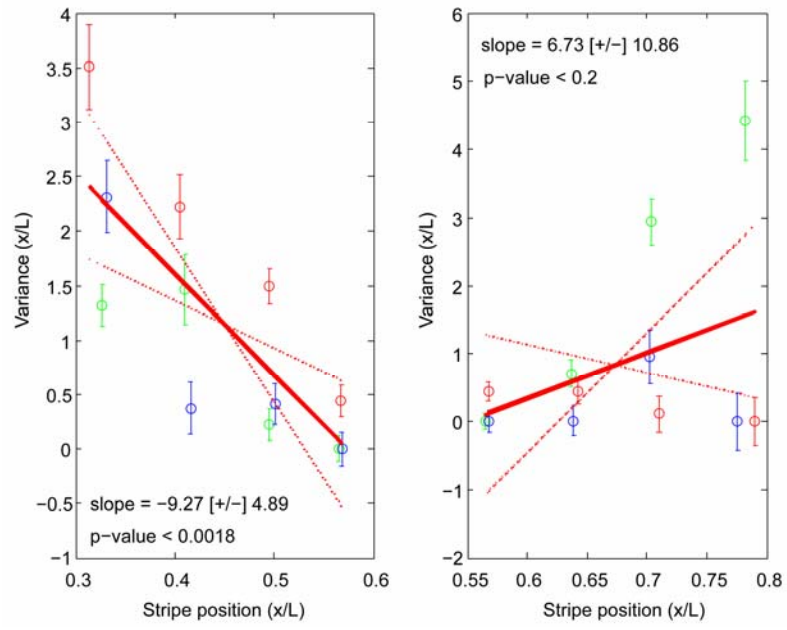

Figure S4. Statistical significance of precision increase from the anterior pole to mid-embryo. Measured variance of the Eve stripes (◦) co-stained with Hb (red), Kr (green) and Gt (blue), for wild-type *bcd* mRNA dosage (c.f. Figure 1), corrected for domain drift and measurement errors. Errors (bars) were estimated by computing the standard deviation across 50 independent (semi-automated) markings of expression domain boundaries. The two linear regressions (red lines) were perfomed to assess statistically if mid-embryo domains are significantly more precise. On the left, the linear regression (performed with data from stripes 1 to 4) shows that the increase in precision towards mid-embryo is indeed highly significant ($p < 0.0018$). On the right, we also observed a trend of increasing precison towards mid-embryo using with data from stripes 4 to 7), however this effect is not very significant ($p < 0.2$) when using the corrected variance.

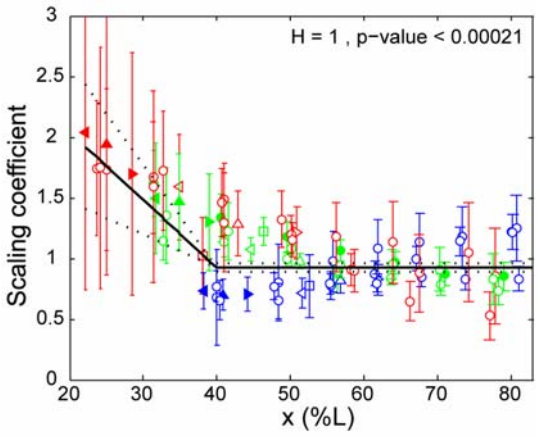

Figure S5. Statistical significance of anterior hyper-scaling. Measured scaling coefficients of the gap and pair-rule gene expression domains as a function of position *x* along the AP axis (see Dataset S2). Errors (bars) represent 68% confidence intervals on the linear regression. For Gt (filled triangles) and Kr (empty triangles), we show results for their left (◁) and right (▷) boundaries, as well as for the center (Δ) of their expression domain. The Hb (□) domain is characterized by the boundary where its concentration drops and the Eve stripes (◦) by the position at which their intensity is maximal (filled circles represent Eve co-stained with Hb, as in A). Color code: 1x*bcd* (red), 2x*bcd* = wild type (green), 4x*bcd* (blue). The linear regression (black line) was performed to assess the significance of anterior hyper-scaling, against a model where scaling is uniform and equal to the weighted mean of the measured scaling coefficients. The p-value was given by an ***F*** test (see text above for more details).

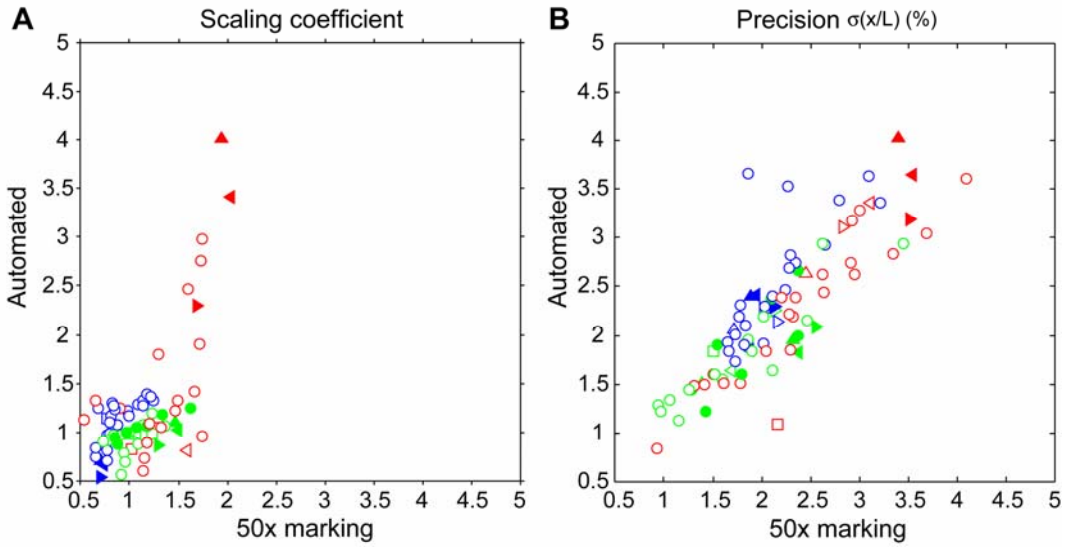

Figure S6. **Scaling and precision with the semi-automated (50x marking) vs automated extration tool.** (A) Scaling coefficients obtained using embryos marked 50 times manually or once automatically. (B) Precision results obtained using embryos marked 50 times manually or once automatically. For Gt (filled triangles) and Kr (empty triangles), we show results for their left (◁) and right (▷) boundaries, as well as for the center (Δ) of their expression domain. The Hb (□) domain is characterized by the boundary where its concentration drops and the Eve stripes (○) by the position at which their intensity is maximal. Color code: 1x*bcd* (red), 2x*bcd* = wild type (green), 4x*bcd* (blue).

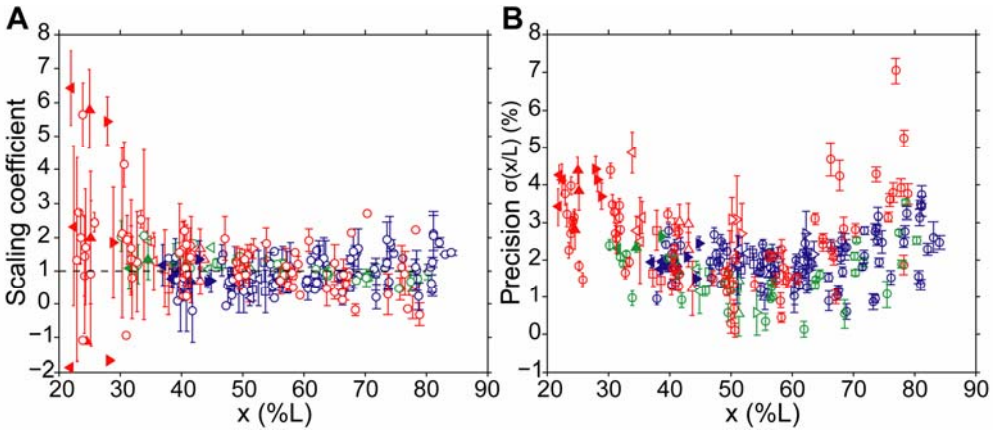

Figure S7. **Scaling and precision of Bcd target genes on different slides.** (A) Measured scaling coefficients of the gap and pair-rule gene expression domains as a function of position *x* along the AP axis, for embryos on the *same* slide (c.f. Equation 7). Errors (bars) represent 68% confidence interval on the linear regression. (B) Measure of precision $\sigma(x/L)$ of the gap and pair-rule gene expression domains as a function of position *x* along the AP axis, for embryos on the *same* slide. Measurement errors (bars) were estimated by computing the standard deviation across 50 independent (semi-automated) markings of expression domain boundaries. For Gt (filled triangles) and Kr (empty triangles), we show results for their left (◁) and right (▷) boundaries, as well as for the center (Δ) of their expression domain. The Hb (□) domain is characterized by the boundary where its concentration drops and the Eve stripes (○) by the position at which their intensity is maximal. Color code: 1x*bcd* (red), 2x*bcd* = wild type (green), 4x*bcd* (blue).

Scaling models

Text S2. *Alternative models for scaling.*

We consider four models that impose a functional relationship between the embryo length and model parameters. For each model, we investigate how the scaling coefficient $S(x,t)$ changes as a function of position and time.

In the first model (Figure S8A, presented in the main text), there is no morphogen degradation at all, such that the external profile never reaches steady state. This extreme case, also considered by (Coppey et al, 2007), assumes that there is no significant morphogen degradation until the decoding time, though it may be triggered latter on. We assume that at the decoding time all embryos have the same number of nuclei independent of their size (which is in good agreement with the deterministic doubling of nuclei at each cycle). Thus the nuclei density *N* depends on the embryo size and we assume that $N \propto L^{-n}$, where $n \in [1;3]$ (here $n=3$ corresponds to a uniform distribution of nuclei, while $n=2$ is true if nuclei are distributed on a shell with a fixed width (Gregor et al, 2007b)). We find that in general, scaling is time- and position-dependent (in Figure S8A, we set $N/K = 8 \cdot \left(L/\bar{L}\right)^{-2}$; see Figure S9 for the dependence of scaling on *N/K* and *n*). Specifically, anterior domain boundaries hyper-scale, in particular if decoding occurs relatively late, while posterior domains show very good scaling for a wide range of decoding times. We note that if there is also cytoplasmic degradation, *S* actually decreases towards zero as we get closer to the steady state, since the length scale is then given by $\lambda = \sqrt{\tilde{D}/\tilde{\alpha}} = \sqrt{D/\alpha}$, which is independent of L, c.f. Equation 6. Importantly, the qualitative behavior of scaling does not depend on the particular value of n (see Figure S9). Therefore, even if the density of nuclei at the embryo surface correlates more weakly with embryo size (Fowlkes et al, 2008), effectively yielding $1 < n < 2$, scaling could still be achieved. Note also that nuclei progressively migrate to the cortex of the embryo, arranged on concentric shells (Foe and Alberts, 1983). At the cortex, nuclei continue dividing, but their radii become smaller (Gregor et al, 2007b). Thus, at each nuclear cycle, it is likely that the ratio N/K does not increase by a factor 2, but much less. For simplicity we therefore considered this ratio to be constant in our simulations and analytical results.

In a second model (Figure S8B), we assume that the effective degradation rate scales inversely with the size of the embryo, i.e. $\alpha = k_\alpha P \propto L^{-p}$, with $p \in [1;3]$. (For example, one may imagine that degradation is performed by a fixed number of proteasomes N_P originally deposited in the embryos which may loose a variable fraction of water, such that the proteasome density P varies between embryos as a function of their length: $P \propto N_P / L^p$.) Interestingly, this model ensures some scaling even at steady state. (We set N/K to zero, to disentangle this effect from scaling due to nuclear trapping.) From Figure S8B, it is apparent that early decoding times show large posterior hypo-scaling, while later decoding times exhibit hyper-scaling even in the posterior-most domains. Specifically, good scaling is only achieved in a small region, which varies as a function of the decoding time. Note that if we consider $p=2$, the steady state length scale correlates perfectly with embryo size, $\lambda \propto L$. However, this is not enough to ensure a scaling coefficient $S=1$ everywhere in the embryo (Figure S10A). This is because the amplitude of the profile, $s_0/\sqrt{\alpha D}$, also depends through α on the embryo size ($\propto L^{p/2}$) and thus, domain boundaries very close to $x=0$ move much more than expected because of the change in amplitude at the source, yielding hyper-scaling.

A third model (Figure S8C) assumes that degradation occurs in the nuclei with rate α_n, as suggested in (Gregor et al, 2007b), yielding an effective degradation rate $\tilde{\alpha} = \dfrac{\alpha_n \cdot N/K}{1+N/K}$. In this model, the morphogen profile converges to a steady state which still exhibits some degree of scaling. For simplicity, we assume that there is no external degradation ($\alpha = 0$) and that the early embryo uses only its nuclear machinery to degrade Bcd. Compared to the simple nuclear trapping model (Figure S8A), it seems that nuclear degradation yields more hypo-scaling in posterior domains, as well as more variability in time. Note that for $N/K >> 1$, scaling results are very similar to those obtained only with nuclear trapping. In this case, increasing nuclear degradation speeds up the convergence to steady state, but does not really change the scaling behavior at decoding time.

Finally, in a fourth model (Figure S8D), the number of ribosomes or the amount of *bcd* mRNA deposited by the mother is assumed to be correlated with embryo size, such that the production rate scales as $s_0 \propto L^s$ (see (He et al, 2008)). In this model, the amplitude of the profile is bigger in larger embryos, giving rise to hyper-scaling in the regions close to the source, as mentionned previously for the second model (in Figure S8D we set $s = 3$ and $N/K = 0$, to avoid scaling due to nuclear trapping). However, this model is less flexible to describe scaling, since the exponent s is its only tunable parameter. Within our parameter constraints to ensure the correct gradient length scale at nuclear cycle 14, this model yields strong hypo-scaling in the posterior domains, in particular at early decoding times.

We also investigated the robustness of scaling when adding 25% Gaussian noise to all the parameters involved in gradient formation (Figure S11). Scaling was robust in all scenarios. However, it appears that the scenarios including nuclear trapping are less sensitive to fluctuations in Bcd decoding time, since the scaling behavior has a similar trend over a large window of times (Figure S8A/C). Moreover, these models show good scaling in most of the embryo, avoiding strong hyper- and hypo-scaling in the anterior and posterior regions, respectively.

While we found that the observed anterior hyper-scaling arises naturally in all the models we considered, only those with nuclear trapping could provide close to perfect scaling in the central and posterior part of the embryo in a manner that is robust to the exact choices of the model parameters, including the onset of patterning. Still, these adhoc models merely serve to provide a proof of principle that the observed scaling pattern can arise naturally, while a more realistic scenario may combine several of their features, as well as other mechanisms that channel information on the embryo size to the morphogen gradient.

In order to fully validate the nuclear trapping models, more experiments should be performed. According to these models, Bcd should not scale at all in the absence of nuclei. This prediction could in principle be tested in unfertilized eggs using our expression for scaling. Yet it would require direct measurements of continuous Bcd concentrations along the gradient (e.g. using a bcd-GFP fusion) for many embryos, which is more difficult than quantification by proxy using its target genes (as we did in this study). Note that if Bcd were not to scale in unfertilized eggs, considering the profiles in relative units (x/L) could be misleading, since the profiles would fluctuate due to the variability in embryo size, in particular in the posterior compartment.

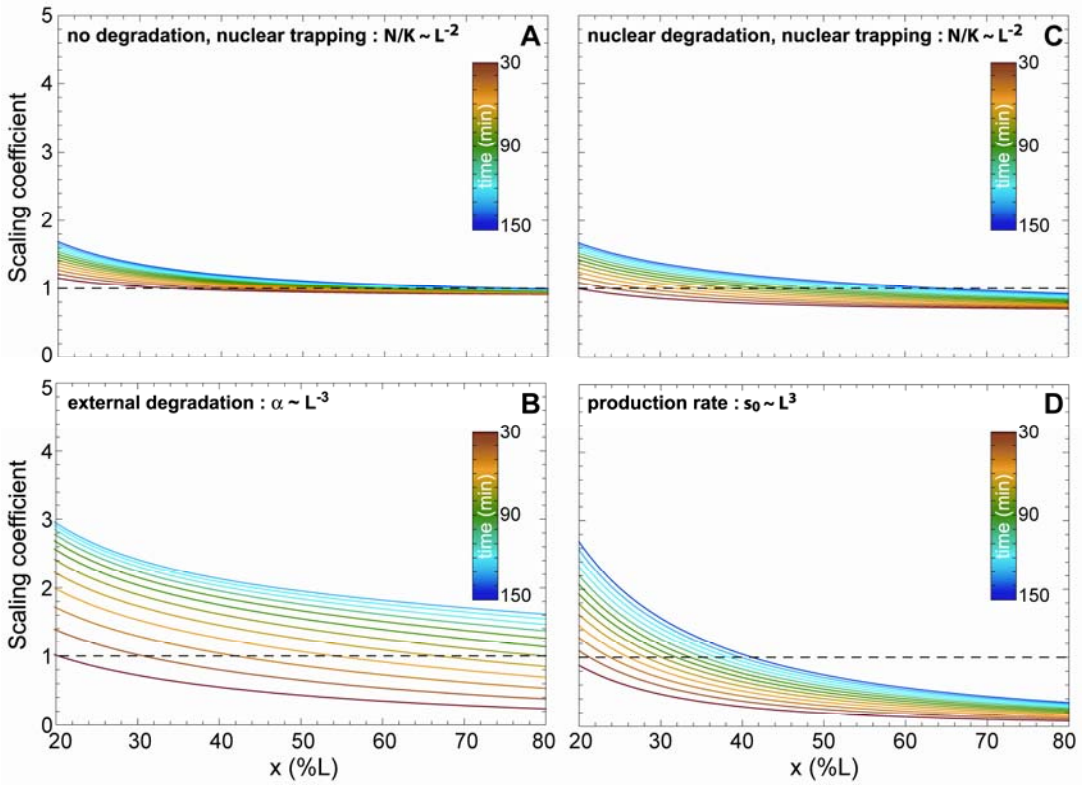

Figure S8. Modeling scaling of Bcd. Parameters are chosen such that the profile is closest to an exponential decay with length scale $\lambda = 0.2L$ at $t = 150\text{min}$ (see Figure S12 for the time evolution). (A) No degradation, scaling is brought about by nuclear trapping, with $N/K = 8\cdot(L/\bar{L})^{-2}$. $D = 12\mu m^2/s$. (B) Degradation is performed by a fixed number N_p of proteasomes, such that their density P scales as $k_\alpha P = 5\cdot 10^{-4}\,\text{sec}^{-1}(L/\bar{L})^{-3}$ (no nuclear trapping). $D = 5.4\mu m^2/s$. (C) Nuclear degradation, $\alpha_n = 3.3\cdot 10^{-4}\,\text{sec}^{-1}$, and nuclear trapping, $N/K = 2\cdot(L/\bar{L})^{-2}$. $D = 8.3\mu m^2/s$. (D) No degradation nor nuclear trapping, scaling appears because the production rate is correlated with embryo size, $s_0 \propto L^3$. $D = 1.5\mu m^2/s$.

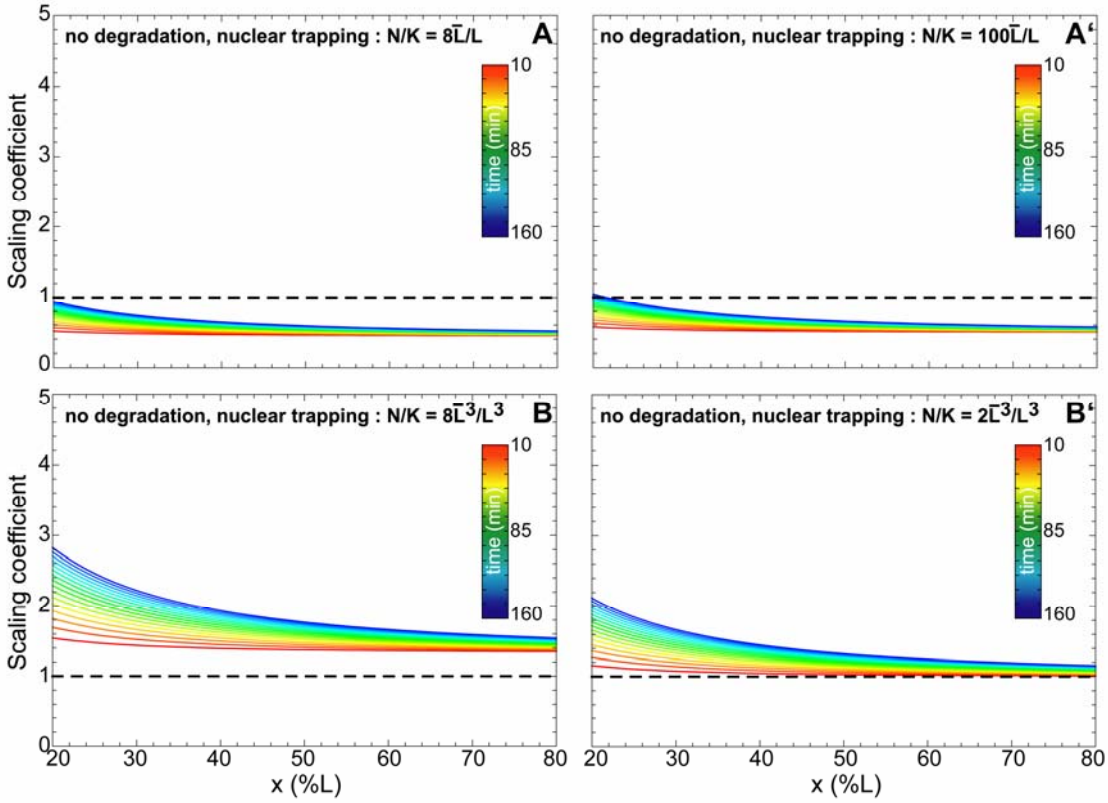

Figure S9. **Modeling scaling of Bcd with nuclear trapping.** Parameters are chosen such that the profile is closest to an exponential decay with length scale $\lambda = 0.2L$ at $t = 100\text{min}$. (A) No degradation, scaling is induced by nuclear trapping, with $N/K = 8\cdot(L/\bar{L})^{-1}$. (A') As in (A), but with $N/K = 100\cdot(L/\bar{L})^{-1}$. With $n = 1$, scaling is position dependent at late times, but too small except for the most anterior region. (B) No degradation, scaling is induced by nuclear trapping, with $N/K = 8\cdot(L/\bar{L})^{-3}$. (B') As in (B), but with $N/K = 2\cdot(L/\bar{L})^{-3}$. Later times exhibit stronger hyper-scaling in the anterior region.

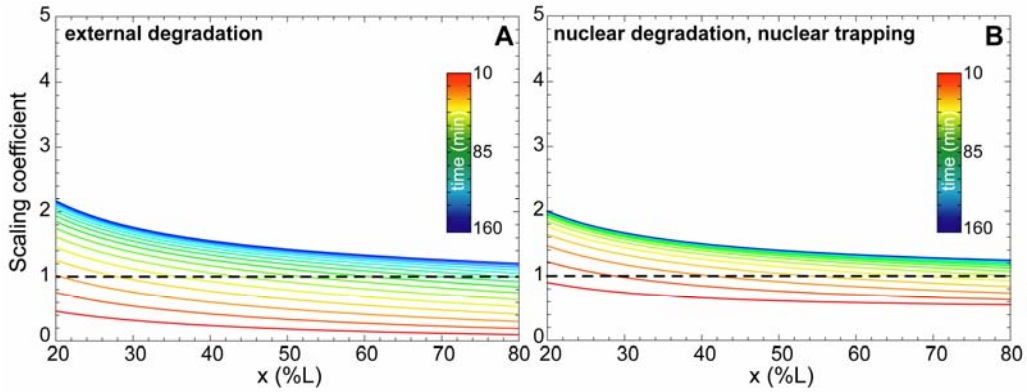

Figure S10. **Modeling scaling of Bcd with degradation.** Parameters are chosen such that the profile is closest to an exponential decay with length scale $\lambda = 0.2L$ at $t = 100\text{min}$. (A) Degradation is performed by a fixed number N_P of proteasomes such that their density P scales as $k_\alpha P = 5\cdot 10^{-4}(L/\bar{L})^{-2}\,\text{sec}^{-1}$ (no nuclear trapping). (B) Nuclear degradation, $\alpha_n = 0.002\,\text{sec}^{-1}$, and nuclear trapping, $N/K = 1\cdot\left(L/\bar{L}\right)^{-2}$.

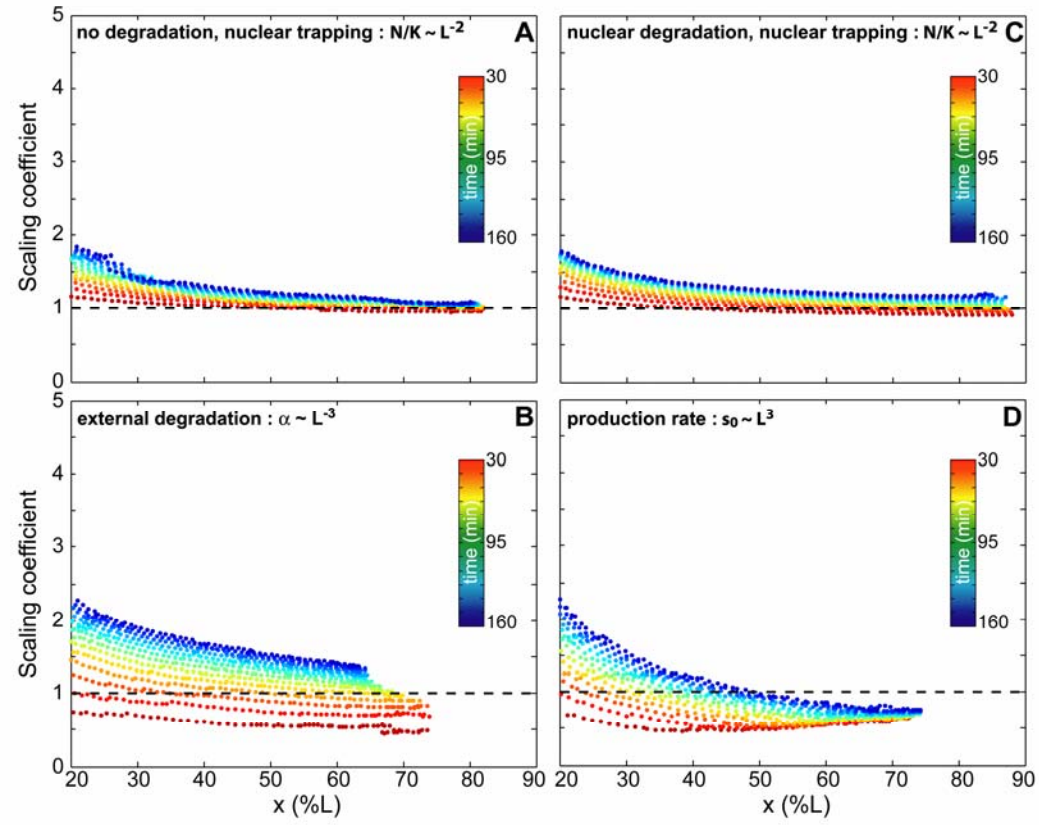

Figure S11. **Numerical results for Bcd scaling in the presence of noise.** Parameters are chosen such that the profile is closest to an exponential decay with length scale $\lambda = 0.2L$ at $t = 100\text{min}$. For many Bcd read-out thresholds, we plot the fluctuations in domain position as a function of the fluctuations in embryo size. The scaling coefficient at each threshold is obtained using Equation 4. 25% Gaussian noise is added to all parameters to test for robustness. (A) No degradation, scaling is brought about by nuclear trapping, with $N/K = 8\cdot\left(L/\bar{L}\right)^{-2}$. (B) Degradation is performed by a fixed number N_P of proteasomes, such that their density P scales as $k_\alpha P = 5\cdot 10^{-4}(L/\bar{L})^{-3}\,\text{sec}^{-1}$ (no nuclear trapping). (C) Nuclear degradation, $\alpha_n = 5\cdot 10^{-4}\,\text{sec}^{-1}$, and nuclear trapping, $N/K = 8\cdot\left(L/\bar{L}\right)^{-2}$. (D) No degradation nor nuclear trapping, scaling appears because the production rate is correlated with embryo size, $s_0 \propto L^3$.

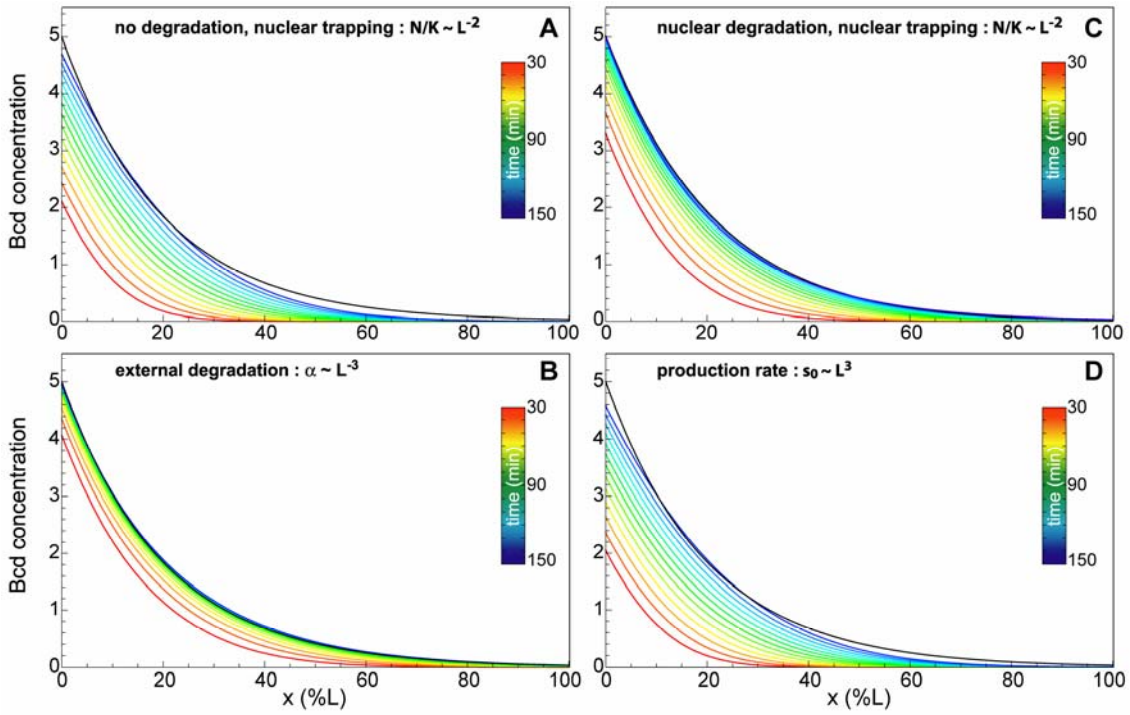

Figure S12. Time evolution of the Bcd gradient for each scaling model. For comparison, a decaying exponential with length scale $\lambda = 0.2L$ is shown in black. (A) No degradation. $N/K = 8\cdot(L/\bar{L})^{-2}$. $D = 12\mu m^2/s$. (B) Degradation is performed by a fixed number N_P of proteasomes such that their density P scales as $k_\alpha P = 5\cdot 10^{-4}\,\mathrm{sec}^{-1}(L/\bar{L})^{-3}$ (no nuclear trapping). $D = 5.4\mu m^2/s$. (C) Nuclear degradation, $\alpha_n = 3.3\cdot 10^{-4}\,\mathrm{sec}^{-1}$, and nuclear trapping, $N/K = 2\cdot(L/\bar{L})^{-2}$. $D = 8.3\mu m^2/s$. (D) The production rate is correlated with embryo size, $s_0 \propto L^3$ (no degradation nor nuclear trapping). $D = 1.5\mu m^2/s$.

Text S3. *Variance induced by imperfect scaling.*

The precision analysis of the gap and pair-rule gene expression domains revealed that precision is maximal at mid-embryo, in good agreement with Bcd precision (Gregor *et al*, 2007). However, we note that imprecision, measured as the standard deviation of the relative domain localizations $\sigma(x/L)$, is impacted both by "internal" noise as well as imperfect scaling. Therefore, in order to differentiate these two contributions, one should take into account that scaling appears to be position dependent (Figure 3B). Assuming that the contributions to the total variance in domain position, $V_{tot} = \sigma_{tot}{}^2$, come from internal noise (V_{noise}) and imperfect scaling (V_{is}) and that these are independent, we have

$$V_{noise} = V_{tot} - V_{is}$$

with (see *Derivation* below),

$$V_{is}\left(\frac{x}{L}\right) = \bar{x}^2\cdot(1-S)^2\cdot V\left(\frac{1}{L}\right). \qquad \text{(S1)}$$

In the regions with perfect scaling ($S = 1$), we have $V_{is}(x/L) = 0$. Thus, considering that Bcd target genes exhibit good scaling in general (Figure 3B), the standard deviation of the relative positions $\sigma(x/L)$ presented in Figure 1 essentially measures internal noise, since $V_{is}(x/L) \approx 0$ (except for the anterior-most region of the embryo).

Derivation of Equation S1

Let us consider a set of embryos of different sizes having mean size $\bar{L}$. We assume that there are only

fluctuations in embryo size and no other internal noises. If all gradients scale perfectly with embryo size, they will look identical on a relative scale, so that the variance at a particular position (x/L) will be zero, $V_{is}(x/L)=0$. Our goal is to estimate the variance in the relative positions of expression domains $V_{is}(x/L)$ due to the imperfect scaling.

According to the definition of *S* in Equation 2 of the main text,

$$\frac{x-\bar{x}}{\bar{x}} = S \cdot \frac{L-\bar{L}}{\bar{L}}.$$

Extracting x/L yields

$$\frac{x}{L} = S \cdot \frac{\bar{x}}{\bar{L}} + (1-S) \cdot \frac{\bar{x}}{L}.$$

Assuming that $S \cdot \bar{x}/\bar{L}$ is constant when L fluctuates, we get Equation S1

$$V_{is}\left(\frac{x}{L}\right) = \bar{x}^2 (1-S)^2 \cdot V\left(\frac{1}{L}\right).$$

We see that for $S=1$ (perfect scaling), there is no variance due to imperfect scaling (i.e. in a relative scale (x/L), all gradients coincide). However, when $S \neq 1$, the variance becomes larger for more posterior expression domains. This means that in the absence of perfect scaling, the imprecision of gradients measured in a relative scale increases towards the posterior pole, even without any internal noise, due to the fluctuations in embryo length.

.

Text S4. *Scaling and correlations.*

In developmental biology, understanding the robustness of gene expression patterns remains a great challenge. In this context, scaling ensures to keep a proportional body plan under the unavoidable fluctuations in embryo or tissue size. The scaling of gene expression domains has often been measured as the correlation of the domain localization with embryo size (Aegerter-Wilmsen *et al*, 2005; Bollenbach *et al*, 2008; Holloway *et al*, 2006; Houchmandzadeh *et al*, 2002; Howard and ten Wolde, 2005). However, perfect correlation is in fact not equivalent with perfect scaling, since it only guarantees a strictly linear response of the domain position with embryo length, but not the preservation of proportions. Thus, correlations are not informative on whether the shift is adequate, or if a specific domain position tends to hyper- or hypo-scale.

Importantly, the scaling measure that we introduced in Equation 5 for continuous gradients and its equivalent for a discrete domain position in Equation 7 not only provides a positional quantification of scaling, but also allows for proper disentanglement of scaling from precision, which is not the case when using correlations. This can be seen readily by writing the correlation in terms of our scaling measure in Equation 4 as

$$\mathrm{corr}(x,L) = S \cdot \frac{\sigma(L)/\bar{L}}{\sigma(x)/\bar{x}}. \qquad \text{(S2)}$$

Thus, the correlation depends explicitly on the fluctuations in the domain position $\sigma(x)$. However, fluctuations in domain position will generally also have a contribution that is not due to fluctuations in embryo size (e.g. internal noise). Consequently, correlations provide a scaling measure that does not properly disentangle such noise from the fluctuations induced by variations in length. Since we have seen that fluctuations in parameters affecting gradient formation give rise to position-dependent imprecision, this is problematic. In contrast, our measure of scaling S only depends on the fluctuations in embryo length $\sigma(L)$ and the covariance $\mathrm{cov}(x,L)$, since the slope was estimated by regressing x on L. Note that the correlation is equivalent to our scaling coefficient only if the mean fluctuation in domain position (relative to the mean domain position) is equal to that of the embryo size (relative to its mean size).

Previous works employed the correlation of the length scale of a (measured) morphogen profile with embryo size as a proxy for scaling (Bollenbach et al, 2008; Gregor et al, 2005). Focusing on the length scale has however several disadvantages: (i) It ignores a potentially position-dependent signal for scaling, (ii) it is only

applicable for profiles that are well-described with a single fixed length scale (like an exponentially decay), and (iii) it does not capture the impact of the morphogen gradient amplitude on scaling. In this work, we have argued that scaling should in general be viewed as a position-dependent feature (c.f. Figure 3) and our measure of scaling introduced in Equations 2-4 can be used for gradients with an arbitrary functional dependence and accounts for the gradient amplitude. Importantly, it provides a unified quantification of scaling for both gradient profiles (c.f. Equation 2 that we used for our modeling approach) and expression domains (c.f. Equation 4 which is the numerical equivalent that we applied to our experimental study). Note that Equation 3 introduces an explicit model for the morphogen gradient interpretation (i.e. the French-flag model (Wolpert, 1969)). Yet, in principle *dx/dL* can be computed also for other, more intricate mechanisms that transmit positional information from the morphogen to its target genes, either numerically or in some cases analytically.

References

Aegerter-Wilmsen T, Aegerter CM, Bisseling T (2005) Model for the robust establishment of precise proportions in the early Drosophila embryo. *J Theor Biol* **234:** 13--19.

Bollenbach T, Pantazis P, Kicheva A, Bökel C, González-Gaitán M, Jülicher F (2008) Precision of the Dpp gradient. *Development* **135:** 1137--1146.

Gregor T, Bialek W, de Ruyter van Steveninck RR, Tank DW, Wieschaus EF (2005) Diffusion and scaling during early embryonic pattern formation. *Proc Natl Acad Sci U S A* **102:** 18403--18407.

Gregor T, Tank DW, Wieschaus EF, Bialek W (2007) Probing the limits to positional information. *Cell* **130:** 153--164.

Holloway DM, Harrison LG, Kosman D, Vanario-Alonso CE, Spirov AV (2006) Analysis of pattern precision shows that Drosophila segmentation develops substantial independence from gradients of maternal gene products. *Dev Dyn* **235:** 2949--2960.

Houchmandzadeh B, Wieschaus E, Leibler S (2002) Establishment of developmental precision and proportions in the early Drosophila embryo. *Nature* **415:** 798--802.

Howard M, ten Wolde PR (2005) Finding the center reliably: robust patterns of developmental gene expression. *Phys Rev Lett* **95:** 208103.

Jaeger J, Surkova S, Blagov M, Janssens H, Kosman D, Kozlov KN, Manu, Myasnikova E, Vanario-Alonso CE, Samsonova M, Sharp DH, Reinitz J (2004) Dynamic control of positional information in the early Drosophila embryo. *Nature* **430:** 368--371.

Surkova S, Kosman D, Kozlov K, Manu, Myasnikova E, Samsonova AA, Spirov A, Vanario-Alonso CE, Samsonova M, Reinitz J (2008) Characterization of the Drosophila segment determination morphome. *Dev Biol* **313:** 844--862.

Wolpert L (1969) Positional information and the spatial pattern of cellular differentiation. *J Theor Biol* **25:** 1--47.